Functional separators for the batteries of the future

Functional separators for the batteries of the future

Antonio Terella[a], Francesca De Giorgio[a], Morteza Rahmanipour[a], Laura Malavolta[a], Elena Paolasini[a], Davide Fabiani[b], Maria Letizia Focarete[a], Catia Arbizzani[a*],
[a]*Alma Mater Studiorum – Università di Bologna, Department of Chemistry "Giacomo Ciamician"*
Via F. Selmi 2, 40126 Bologna (Italy)
[b]*Alma Mater Studiorum - Università di Bologna, Department of Electric, Electronic and Information Engineering "Guglielmo Marconi"*
Via Risorgimento 2, 40136 (Italy)

**Corresponding Author: catia.arbizzani@unibo.it*

Abstract

Lithium/sulfur batteries are one of the most promising technologies for the next-generation batteries. However, this technology suffers from several problems mainly related to the instability of metallic lithium and to the polysulfides (PS) shuttle. An approach to address such issues is the design of new separators or the modification of existing commercial ones.

The use of hybrid membranes is here proposed to improve the performance of Li metal anode and sulfur cathode. Composite separators are obtained by electrospinning or drop-casting a polymer solution of polyvinylidenefluoride (PVdF) containing graphene oxide (GO) on a polyolefin commercial Celgard 2300 separator. This is the first time that a thin layer of electrospun PVdF/GO composite is applied to a polyolefin separator for the use in Li metal-based batteries. We demonstrate that electrospinning is an effective method to obtain a thin polymer layer of PVdF/GO. The electrospun layer improves the wettability of the separator; it is beneficial to the growth of "soft" dendrites on Li anode and has a positive effect on the PS shuttle process. The casted layer featuring a higher GO content is also effective in increasing the separator wettability, although with a minor effect on Li interphase.

Keywords: electrospinning; functional separator; interphase; lithium; PVdF/GO

1 Introduction

Even if the separator has been considered so far an inactive component of a battery, its properties are of paramount importance for the operation and safety of batteries featuring liquid electrolyte. It avoids the contact of the electrodes and prevents electronic short circuits while enabling ion transport. Its mechanical, chemical and electrochemical stability assures long life to the device and its thermal stability may act as a switch to shut down the current flow in case of battery overheating. The thickness and the amount of soaked electrolyte affect the specific and volumetric device performance [1, 2].

The increasing energy demand and the wide spread of renewable energy sources requiring large-size, safe and low-cost energy storage systems have driven the research efforts on the so-called post lithium-ion batteries that include Li-metal batteries, Li/S, metal/air and Na-ion batteries.

However, these batteries have some issues to be overcome. In Li/S batteries, polysulfides (PS) are produced during the discharge. The long-chain PS that are formed near the cathode are extremely soluble in organic electrolytes, diffuse through the separator and reach the lithium anode. They are reduced to short-chain PS and to insoluble Li_2S. The short-chain PS re-diffuse towards the cathode and can be further oxidized [3, 4]. This process involves a loss of active material, and in turn a decrease of cell capacity during the operating cycles, and a deleterious effect on Li metal.

In metal/air batteries, the oxygen crossover can take place. The O_2 molecules diffuse through the separator and reach the lithium metal electrode, inevitably leading to a direct chemical reaction. This causes a self-discharge and a decrease of battery capacity, and have a negative impact on the safety of the system [5]. Recent studies have highlighted that separators should accomplish also other functions, i.e. blocking lithium polysulfides in Li/S batteries, blocking O_2 and moisture in Li/air batteries, contributing to the formation of a smooth Li surface avoiding the formation of dendrites in batteries with metal Li anode [6-11]. In addition, the demand for low-cost, environmentally-friendly Na-ion batteries for the large-scale use of renewable energy requires an eco-efficient fabrication of sustainable separators [12].

Several strategies have been pursued to create new separators or to modify commercial ones in order to have membranes that actively contribute to the operation of the battery, by adding carbonaceous particles, metal oxides, ionomers and polymers into the separator structure or by forming a surface layer [13-16]. In the present work, we report the physico-chemical properties and the electrochemical performance of electrospun and drop casted polyvinylidenefluoride (PVdF)/ graphene oxide (GO)/polyolefin composite separators as active components for both Li metal and sulfur-based electrodes.

Different approaches have been adopted so far to modify separators, including the use of the electrospinning technique. Electrospinning is widely used in energy materials field for the production of new generation nanofiber separators [17-19]. It allows the creation of polymeric fibers with diameters of the order of tens of hundreds of nanometers. The obtained fibers can create non-woven mats or can be deposited on a substrate by making thin coating with high surface area [20, 21]. Fiber diameter, spatial distribution and thickness of coatings can be controlled by setup parameters such as time of electrospinning, type of collector, voltage and syringe-collector distance and needle diameter [22]. PVdF is the most widely studied polymer for battery separators [23-25] thanks to its high electrochemical stability, high dielectric constant and full compatibility and

adhesion with the electrodes that contain PVdF binders. It can also be easily electrospun or drop casted from solutions [16, 19]. The "soft" PVdF surface in contact with Li metal electrode may positively affect solid electrolyte interphase (SEI) formation with the suppression, or at least the decrease, of the dendrite formation, due to a higher electrolyte uptake and better Li wettability [26, 27]. In terms of PS permeability, graphene oxide (GO) has been demonstrated to be effective in producing perm-selective membranes for lithium/sulfur batteries given the negative charge that facilitates Li ion permeability and hinders anion crossover by electrostatic repulsion and steric hindrance [28, 29]. Electrospun composite membranes containing PVdF and GO have been studied only for water filtration and treatment [30]. By excluding a study on GO/Nafion coating on polyethylene separator [31] and a study on electrospun PVDF-co-CTFE nanofiber coated on polyolefin [32], to the best of our knowledge this is the first time that a thin layer of electrospun PVdF/GO composite is applied to a separator for use in Li metal-based batteries.

2 Experimental

2.1 Separators preparation

Commercial three-layer polypropylene (PP)/polyethylene (PE)/PP membranes (Celgard® 2300, thickness: 25.4 μm, porosity: 37%) have been modified via graphene oxide (GO, Nanoinnova technologies) and polyvinylidene difluoride (PVdF, Solef 6008, Solvay). The electrospinning process has been carried out to produce a very thin layer of electrospun nanofibers on one side of the commercial separator, simply indicated as Celgard, which has been placed between the needle and the collector. The experimental conditions have been based on our previous works [16, 19]. The electrospinning apparatus consisted of a syringe pump (KDScientific), a glass syringe, a stainless-steel, blunt-ended needle (0.31 mm internal diameter) connected to a high voltage power supply (Spellman, SL 50 P 10/CE/230) and a grounded cylindrical rotating collector. The polymer solution based on PVdF 15 w/v % in acetone: dimethylsulfoxide 70:30 (v/v) and GO 0.5 w/v % was dispensed from the needle placed 15 cm apart from the collector. The electrospinning process was carried out in a glove box at room temperature and relative humidity of 40–45% with a solution flow-rate of 0.45 mL h^{-1} and 18 kV-applied voltage. Varying electrospinning durations of 5, 10 and 15 minutes were considered to optimize the coating thickness. The samples were named as E1, E2, and E3, respectively, with a coating ranging from less than 30 μm to 40 μm. The amount of GO on the separator (ca. 4 μg cm^{-2}) was estimated from the weight of the electrospun layer by considering that all the GO was uniformly distributed in the nanofibers. In order to obtain a higher amount of GO in the modified separator, a casting procedure has been carried out by using three solutions containing a total amount of 8 w/v % of the two components (PVdF and GO, respectively, 7.9 and

0.1, 7.8 and 0.2, and 7.5 and 0.5 w/v %). PVdF and GO were alternately dissolved in acetone under stirring at 40°C for 30 min. Thereafter, the solution was sonicated for 1 hour to promote GO dispersion. The solutions (1.5 mL for each separator) were then deposited on Celgard by using a mini coater (Mini Coater MC-20, Hohsen Corp.). The rolling bar height was kept at 0.076 mm (3 mil) and the scan speed was set at 0.9 cm s^{-1}. The casting procedure was also performed on Celgard pretreated in ethanol for 15 min. The samples were named S1C, S2C, S5C and S1CT, S2CT, S5CT, where the numbers 1, 2 or 5 indicate the GO percentage (0.1%, 0.2%, and 0.5%, respectively) and the letter T indicates ethanol treatment of Celgard before carrying out the deposition and casting of PVdF/GO solution. The amount of GO was estimated to be in the order of 2-40 μg cm^{-2} in the samples obtained by casting PVdG/GO suspensions and the composite separator thickness was in the range 30±2 μm for all the samples.

The modified separators were dried under vacuum in a Büchi B-585 Kugelrohr at 80°C for 2 hours in order to remove any trace of residual solvent and humidity and transferred in an argon-filled MBraun Labmaster SP dry box (< 0.1 ppm H_20, < 0.1 ppm O_2) for use.

2.2 Physico-chemical characterization

FTIR-ATR spectra were collected by a Bruker Alpha spectrometer between 4000 and 400 cm^{-1} (4 cm^{-1} resolution) and scanning electron microscopy (SEM) by a Zeiss EVO 50 microscope equipped with an energy dispersive X-ray analyzer from Oxford INCA Energy 350 system.

Test of the dielectric strength of Celgard membranes before and after the electrospinning process were carried out to evaluate the ageing effect of the high voltage applied for the formation of the PVdF electrospun fibers. The tests were carried out with a Bauer DPC tester. The specimen was placed between two metal spheres immersed in paraffin oil. The voltage between the electrodes has been increased and the voltage at which a disruptive discharge takes place (voltage breakdown) has been detected. Each test was repeated 10 times. The results were then analyzed using the Weibull probability function.

The electrical conductivity tests were performed at 45°C and at 70°C on samples modified by casting procedure and containing different amounts of GO (4 and 40 μg cm^{-2}) to evaluate the GO effect. The tests were carried out by a Keithley 2290E apparatus of 5 kV as described in Ref. 16. The applied voltage between the electrodes was 200 V and the separator thickness was 25.4 μm for Celgard and 30 μm for the modified ones. The area of the electrodes was $5.726 \cdot 10^{-4}$ m^2 (27 mm diameter). The charging current flowing through the separators was measured until the steady-state conduction current was reached. The electrical conductivity (in S m^{-1}) was evaluated as $\sigma = I\ d\ /\ V \cdot S$ where V is the DC applied voltage (in V), S is the electrode area (in m^2), d is the distance

between electrodes, i.e. the separator thickness (in m) and I is the current (in A). The electronic conductivity of the samples was very low (in the range 3-10·10^{-16} S m^{-1} at 45°C and 35-160 ·10^{-16} S m^{-1}at 70°C) even by increasing ten times the amount of GO.

The resistivity of the electrolyte-soaked membranes was measured by electrochemical impedance spectroscopy (EIS) using a Solartron SI 1255 frequency response analyzer coupled with an EG&G Model 273A PAR and Biologic VSP potentiostat/galvanostats. For EIS analysis, the separator previously soaked with the electrolyte was placed in a T-shaped Teflon cell (BOLA by Bohlender GmBH) between two stainless steel (SS) blocking electrodes (0.785 cm^2) in a symmetrical configuration. The cell was kept in a Memmert IPP 200 incubator at 30 °C and the measurements were performed after one hour to allow system stability to be achieved. EIS measurements were carried out by applying an AC perturbation of 5 mV with a variable frequency from 200 kHz to 100 mHz, collecting 10 points per decade. The MacMullin numbers were calculated by $N_M = \rho_s/\rho_e$ where ρ_s is the resistivity of the electrolyte/separator assembly under study and ρ_e is the resistivity of the electrolyte [33, 34]. The electrolytes were ethylene carbonate: dimethyl carbonate 1 M $LiPF_6$ (LP30, Selectilyte, BASF) and 1,3-dioxolane (DOL, > 99.8%, Sigma-Aldrich): 1,2-dimethoxy ethane (DME, > 99%, Sigma-Aldrich) 1:1 v/v – 1 M lithium bis (trifluoromethanesulfonyl)imide (LiTFSI, > 99.95%, Sigma-Aldrich) – 0.1 M $LiNO_3$ (≥ 99.99%, Sigma-Aldrich). Hereafter, the electrolyte solutions are indicated as LP30 and DD.

A solution of Li_2S_8 was prepared by mixing Li_2S (Li_2S, ≥ 99.98%, Sigma-Aldrich) and S (≥ 99.99%, Sigma-Aldrich) in stoichiometric amounts in DOL:DME 1:1 v/v and stirring for 48 hours at 70°C. Permeability tests were carried out by using a glass tube that was closed on one side by the membrane under test, fixed to the tube by a Teflon O-ring. The tube, filled with 1 mL of nominal 0.5 M Li_2S_8 in DOL:DME 1:1 v/v, was immersed in 2 mL DOL:DME solution so that the levels of the two liquids coincided. UV-VIS spectra were collected with a Perkin Elmer Lambda 19 with quartz cuvettes.

2.3 Electrochemical tests

BOLA cells in three-electrode configuration with a Li reference electrode (RE) were assembled for the study of Li/separator interface in DD. Galvanostatic charge and discharge cycles were carried out on symmetric Li//Li cells at a current of ± 0.75 mA cm^{-2} for 1 hour. EIS spectra from 100 kHz to 100 mHz (5 mV AC, 10 point/decade) were also collected at the beginning and at the end of the galvanostatic test in open circuit condition.

Li/PS cells were assembled in two-electrode configuration in El-Cell (ECC-Std, El-Cell) using a current collector based on Kynol carbon electrode (Kynol ACC507-15, Kynol Europa, 1500 m^2g^{-1})

(1.77 cm^2) soaked with 70 µL of the solution 0.5 M Li_2S_8 in DOL:DME 1:1 v/v - 0.25 M LITFSI – 0.1 M $LiNO_3$. The S loading was 5 mg cm^{-2} [35, 36].

Sulfur-based cathodes were prepared by using a carbon previously impregnated with sulfur (S/C), with S:C= 4:1 as reported in Ref. [34]. The electrode, containing 87.4 wt.% S and 4.6 wt.% carbon black (Ketijen Black, Akzo Nobel) and 8% PVdF (KynarvHFV, Archema) was prepared by dry mixing in a mortar S/C and carbon powders and by adding the solids to a solution of PVdF in N-methylpyrrolidone (NMP). The electrode sulfur content was 70%. The slurry was stirred for 5 hours and was finally spread on a KOH-etched Al current collector by means of a Mini Coating Machine (Hohsen Corporation) at 0.3 cm s^{-1} and with a bar distance of 8 mil. The galvanostatic charge/discharge cycles were performed in BOLA cells in three-electrode configuration to monitor the electrode potentials even if an excess of DD electrolyte was required to ensure the lithium RE contact. The counter electrode (CE) was a lithium disk. Tests of Li/S-C cells were also carried out in two-electrode configuration with 40 µL of DD electrolyte to evaluate the performance of different separators upon galvanostatic charge/discharge cycling at C/10-rate. The cathode sulfur loading was ca. 2 mg cm^{-2}.

All the electrochemical tests were carried out with a Biologic VSP potentiostat/galvanostat at 30°C.

The contact angle experiments were carried out with propylene carbonate (PC) solvent using a Theta Lite Instrument (Biolin Scientific) and collecting 20 images s^{-1} for 10 s.

3 Results and discussion

3.1 Separator preparation and physico-chemical characterization

Several PVdF/GO coatings were obtained on Celgard separators with different electrospinning durations, from 5 to 15 minutes. The coating thickness ranged from < 5 to 10 µm and the best adhesion to the Celgard separator was obtained with the thinnest layer (5 minutes spinning, < 5 µm). A mild pressing procedure (200 psi, 70°C, 1h) was performed on E1 separators since it was necessary to maintain the adhesion of the thicker layers. The pressed separators were indicated as E1p.

Figure 1 shows the SEM images of the sample E1 (5 min spinning). The random distribution of the fibers and the absence of defects are noticeable. The fiber diameters range between 0.6 e 0.9 µm. Figure 1d shows the PVdF/GO coating manually detached from the Celgard layer and Figures 1e and 1f display the cross-sections of the modified separator.

Figure1

In order to verify if ageing phenomena of the supporting Celgard membrane occurred due to the exposure to strong electric fields during electrospinning, the dielectric strength tests were performed on the composite PVdF/GO/Celgard E1 membrane and on the Celgard membrane after PVdF/GO layer was peeled off. The results are compared with the pristine Celgard separator and displayed in Figure 2. The Figure shows that the average value of the voltage at which the breakdown occurs is lower for E1 membrane due to the tip effect created at the edges of the GO particles where the electric field is locally more intense. The voltage back to being comparable to that observed for the pristine Celgard after the PVdF/GO layer was peeled off. The lower value is attributed to the possible residues of GO on the Celgard surface. The results demonstrated that there are no aging phenomena due to the high electric fields applied during electrospinning.

Figure 2.

Figure 3a shows the FTIR-ATR spectra of PVdF/GO/Celgard separator with 0.1% GO obtained by casting procedure (S1CT), and of the pristine Celgard. It is evident that coverage occurs. Indeed, the typical Celgard peaks near 2900 cm^{-1} (CH_2 and CH_3 stretching vibrations) decrease in intensity, as well as the peak at 1404 cm^{-1} that can be assigned to CH_2 wagging vibration. The peak associated to C–C–C asymmetrical stretching vibration and C-F stretching vibration, are at 878 and 840 cm^{-1}, respectively. The bands at 1180 cm^{-1} and 1250 cm^{-1} are mainly due to the CF_2 symmetric stretching peaks. There exist several peaks below 800 cm^{-1} several peaks which are ascribed to CF_2 bending and wagging modes [37]. In the range 1060-1280 cm^{-1} there are also the peaks related to C-O-C bending and C-C and C-O stretching vibrations of the graphene oxide.

Figure 3.

To evaluate the contribution of the membrane to the cell resistance, the dimensionless parameter of MacMullin (N_M) has been evaluated by EIS measurements as described in the Experimental Section. Figure 4 shows the EIS spectra of some selected separators and Table 1 shows the N_M values of pristine Celgard and of the modified membranes soaked with LP30 electrolyte and with DD electrolyte. While E1, S1C, and S2C show N_M values on a par with to that of pristine Celgard and the effect of GO seems negligible, the separators with the treated Celgard display higher values.

Figure 4.

Presumably, ethanol pretreatment promotes the opening of the pores of the separator and facilitates the access of the PVdF/GO during the deposition procedure that counters the effect of pore opening, producing an increase in ionic resistivity. PVdF/GO occludes the pores and porosity decreases. Besides the increase of the resistivity, the separators with pretreated Celgard could positively affect the performance of the composite separator obtained by casting procedure in blocking, at least in part, the polysulfide shuttle process.

The sample with 0.5% GO displays different behavior. The effect of the treatment is reversed, and a lower N_M is found. In this case the great amount of GO, also visible to the eye, greatly helps the wettability thus improving ion transport to the separator.

Table 1

N_M should be quite independent of the electrolyte. However, the N_M values obtained by using DD instead of LP30 were almost halved, thus indicating that the viscosity of the electrolyte affects this parameter. The lower viscosity of the DD electrolyte allows a better wettability, which apparently decrease the effect of separator tortuosity, being N_M also defined by the ratio of the square of the tortuosity and the porosity.

The slightly lower N_M value of E1p with respect to that of E1 is probably due to the more uniform surface stemming from the pressing process, accounting for a better and uniform wettability. The contact angle tests (Figure S1) confirmed the increased wettability of the separator by means of the PVdF/GO layer, especially increasing the GO amount.

Polysulfide permeability tests were carried out as described in the Experimental Section. The initially transparent solution in which the tubes containing polysulfides were immersed became colored after 1 minute, thus suggesting that polysulfides are not totally blocked by the modified membrane. However, the color is less intense than with the pristine Celgard even after 1 hour. Figure 5 demonstrates the UV-VIS spectra of the DOL:DME solution after polysulfides permeation through the S1CT and Celgard membranes.

Figure 5

The long-chain polysulfides S_6^{2-} and S_8^{2-} should show absorption peaks at 470 and 580 nm, respectively [38]. These absorption peaks are not clearly visible due to the instability of long-chain polysulfides in DOL:DME, specifically in highly diluted solutions. Short-chain polysulfides like S_4^{2-} should be detected at 420 and 320 nm, and $S3^{\bullet-}$ at 617 nm. The latter could be responsible for

the broad absorption between 600 and 700 nm that is evident only in the solutions permeated from Celgard.

3.2 Electrochemical characterization

To investigate the stabilinzing effect of the PVdF/GO electrospun-modified Celgard on stabilizing Li metal interphase in DD electrolyte, we assembled symmetric Li//Li cells where the electrospun layer was placed toward the working electrode (WE) and symmetric Li//Li cells where it was placed toward the counter electrode (CE). We also examined symmetric cells wherein two separators were coupled.

Deposition/stripping tests were carried out on cells with 6 separator configurations in three-electrode mode: Celgard, E1, E1p, 2-E1, 2-E1p, C-E1p. The last three configurations comprise two separators. In 2-E1 and 2-E1p configurations, two equal separators, E1 or E1p, were placed with the electrospun layers faced toward the WE and the CE. In C-E1p configuration, the E1p and pristine Celgard separators were placed with the electrospun layer in between. This configuration, in which both electrodes are in contact with the bare Celgard, has a PVdF/GO core that can entrap the polysulfides by maintaining the electrode in contact with bare Celgard.

Figure 6 shows the potential profiles of the WE and the CE electrodes during galvanostatic stripping/deposition cycles at 0.75 mA cm^{-2}. The duration of each cycle was 2 hours (1-hour charge and 1-hour discharge), and the cut-off potentials of the electrodes were set to -0.5 V and 0.5 V vs. Li^+/Li. The cell voltage profiles are reported in Figure S2.

Figure 6.

Figure 6a displays the overpotential values of the WE and the CE in the cell with Celgard separator. The values are close to 30 mV and decrease to 10 mV due to the formation of dendrites that determine the increase of the surface area. The separator E1 (Figure 6b), with the electrospun layer toward the WE, displays a symmetric deposition/stripping process at the WE. On the other hand, a great overpotential asymmetry is observable at the CE, indicating that the electrospun layer assures a better wettability to the WE rather than of the CE. However, some spikes indicate the occurrence of pinpoint short circuits [39, 40]. The small, localized contact between electrodes can be self-corrected. Indeed, the pinpoint short circuit locally increases the temperature and the small regions in contact melts and shut down the current in that point without compromising the overall cell operation. The application of a light pressure to the E1 separators improved the performance and the cycle stability as shown in Figure 6c. The better symmetry in the deposition/stripping of the WE

evinces a better uniformity of the electrospun layer of E1p. The CE displays, as in the previous cases, the oxidation overpotential higher than the reduction one, indicating that the stripping process is more hindered. This could be ascribed to the formation of a passivation layer during Li deposition.

The use of combined separators confirms that the electrospun layer positively affects the electrode/electrolyte interphase. The potential profiles of 2-E1 cell in Figure 6d, with two separators featuring non-pressed electrospun layers facing the electrodes, confirm the non-optimal morphology of the separator (as per Figure 6b) even if there is a good symmetry between the oxidation and the reduction values of both WE and CE. The 2-E1p cell (Figure 6e), with the same configuration but with the pressed E1 separators, is the best and the most stable one, with the overpotentials of both electrodes which are very similar up to 100 cycles. Figure 6f displays a gradual decrease of the overpotential, which was initially very high, probably due to the insufficient wettability of the separator in the first cycles. Indeed, in C-E1p the electrospun layer is sandwiched between the two Celgard layers. As observed in Figure 6a, the system is quite stable, and the overpotential is approximately 40 mV. Figure S3 shows the potential profiles of the first five and the last five final cycles of the cells shown in Figure 6.

Figure 7 depicts the initial and final spectra of the symmetric Li//Li cells assembled with 2-E1, 2-E1p and C-E1P whose cycle tests are reported in Figures 6d, 6e and 6f, respectively. In these cells, the interphases of the two electrodes are identical: in the first two cells, the electrospun layer is in contact with the electrodes and in the third cell the layer on E1p is internal and the PP is in contact with the two electrodes.

The Nyquist plots, collected in open circuit potential conditions, show two semicircles. The semicircle at high frequency, which starts at the R_b value due to the ionic conductivity of the DD electrolyte, is attributed to the grain boundaries in SEI. The semicircle at low frequency is due to the charge transfer process. The sum of R_{SEI} and R_{ct} is the total electrode resistance (R).

The cell with 2-E1p separator display initial R_{SEI} and R_{ct} values lower than those of 2-E1, owing to the more uniform wettability of the pressed layer. On the contrary, the values of R_{SEI} and R_{ct} of the cell with C-1Ep are almost double implying that the electrospun layer provides a better interphase contact. However, after 200 hours of galvanostatic cycles, all spectra revealed a drastic impedance decrease, suggesting Li dendrite growth. As an effect, the total resistance values become of the order of tens of ohm, the resistance of the cell with C-E1p being the highest one. At the end of cycles lithium electrodes are dark grey and porous on the separator side, displaying the growth of thin dendritic agglomerates that dramatically increase the resistance of the electrode.

The electrochemical results of Figures 6a-6f and the impedance spectra of Figure 7 suggest that the

contact between the electrospun layer and the Li electrode is beneficial for the Li deposition/stripping processes. The different morphology of the Li surface faced to the electrospun PVdF/GO layer and of the Li surface faced to Celgard, evidenced in the SEM images of Figure 8a and 8b, confirms these results. The random distribution of fibers in the electrospun polymer layer hampers the preferential direction of Li-dendrites growth and produces big and smooth dendrites. On the contrary, the homogeneous and highly oriented structure in Celgard separator facilitates the Li dendrites formation on preferential paths. A possible description of the "soft" dendrites growth is shown in Figures 8c and 8d.

Figure S4 shows the SEM images of pristine Li electrode and of the separator side with the electrospun polymer layer after deposition/stripping tests performed in Li//Li cells.

Figure 7.

Figure 8

The effect of E1 and S5C separators on the performance of a PS-based cathode was investigated. The cathode was made of a carbon fabric electrode on which 70 μL of a solution of PS was placed (see Experimental part for the details). Hence, 100 μL of a DD solution was placed on the separator and a Li anode was inserted to complete the cell.

Preliminary results are shown in Figure 9 that compares the voltage profiles of cells with E1 and S5C separators with those of a cell with Celgard separator. The cell featuring E1 separator shows higher specific capacity than the cell with separator prepared by casting procedure. However, the coulombic efficiency is low, even after only 10 cycles. The cells with the separators modified by casting procedure displays decreased capacity but increased coulombic efficiency, probably for the better uniformity of the separator surface, confirming the effect of GO in hindering the PS shuttling. The effect of the PVdF/GO layer, whatever is electrospun or casted, in presence of PS is mainly produced on cathode interphase, and it is not a bulk effect. Figure S6 shows the voltage profiles of Li/PS cells in which the layer is faced to the cathode compared to those in which the layer has been faced to the lithium electrode. It is clearly seen that the layer facing the lithium electrode is less effective on PS shuttling.

Figure 9.

The E1p separator was also tested in a cell with a sulfur-based cathode to prove the effect of the electrospun PVdF/GO layer in presence of a lower amount of PS, which have been formed at the

cathode during the discharge process. Figure 10 represents the potential profiles of the anode (black) and of the cathode (red) during the first 3 cycles of the cell with E1p with the electrospun layer faced to Li anode. During cell charge, the first peak in the anode overpotential could be attributed to the difficulty in deposit fresh Li on a surface covered by the passive layer that is formed when lithium comes in contact with the electrolyte. The overpotential increases at the end of the charge. During the discharge, the anode overpotential increases after the first plateau where Li_2S_6 formed, remains constant during the formation of Li_2S_4 and increases again in the final stage of the cell discharge, when the formation of Li_2S_2 and Li_2S occurs.

Figura 10.

This test clearly evinces that the anode immediately senses the presence of short-chain PS and of their reaction products even in presence of low PS concentration. The increase of the stripping overpotential, which is higher than the deposition overpotential, indicates that the formation of a thick passivation layer that hinders lithium dissolution occurs. Galvanostatic charge/discharge cycles have been performed on Li//S-C cells in two-electrode configuration with E1, S5CT and Celgard at C/10 C-rate to evaluate the performance of the separator over cycling. Although the cell performance is not optimized and affected by the presence of PS, Figure S7 confirms that the PVdF/GO electrospun layer has a positive effect on cell stability. This effect is more evident than that of PVdF/GO casted layer.

4 Conclusion

We have demonstrated that electrospinning is an effective method to modify commercial Celgard separator with a thin polymer layer of polyvinylidene difluoride/graphene oxide (PVdF/GO) that improves electrode/separator interphase in next-generation Li metal batteries. The chemical-physical and electrochemical properties of the electrospun-based separator are comparable to those of PVdF/GO-modified ones obtained by a casting procedure. The electrospun layer improves the wettability of the separator and it is beneficial to the growth of “soft” dendrites on Li anodes thanks to the random distribution of fibers that hampers the preferential direction of Li-dendrites growth. The electrochemical performance of Li//PS and Li/S-C cells demonstrated that the electrospun PVdF/GO layer is also viable in mitigating the PS shuttle even if not very effective. The casted layer is less effective in increasing the separator wettability and in mitigating PS shuttle phenomenon, and has a minor effect on Li interphase. The separator modified by an electrospun layer can thus be suitable for all the devices that use Li metal anodes, like the next generation Li

batteries.

Acknowledgments

The research was funded by Regione Emilia-Romagna Bando Alte Competenze, by CAT Progetti S.R.L and by MiSE-ENEA Electrical System Research "Energy storage for electric system" Project. The Authors would like to thank CAT Progetti S.R.L. for providing electrospinning equipment and P. Bertuzzi (CAT Progetti S.R.L.) for the helpful discussions.

References

[1] S. S. Zhang, J. Power Sources 164 (2007) 351-364.

[2] X. Huang, J. Solid State Electrochem. 15 (2011) 649-662.

[3] D. Bresser, S. Passerini, B. Scrosati, Chem. Commun. 49 (2013) 10545-10562.

[4] Y. V. Mikhaylik, J. R. Akridge, J. Electrochem. Soc., 151 (2004) A1969-A1976.

[5] R. S. Assary, J. Lu, P. Du, L. Xiangyi, X. Zhang, Y. Ren, K. Amine, ChemSusChem, 6 (2012) 51-55.

[6] W. J. Kwak, J. Park, T. T. Nguyen, H. Kim, H. R. Byon, M. Jang, Y. K. Sun, J. Mater. Chem. A, 7 (2019) 3857-3862.

[7] X. Zhang, Z. Xie, Z. Zhou, ChemElectroChem, 6 (2019) 1969-1977.

[8] S. H. Lee, J.- B. Park, H.- S. Lim, Y.-K. Sun, Adv. Energy Mater. 7 (2017) 1602417 (1-6).

[9] B. G. Kim, J.- S. Kim, J. Min, Y.- H. Lee, J. H. Choi, M. C. Jang, S. A. Freunberger, J. W. Choi, Adv. Funct. Mater. 26 (2016) 1747-1756.

[10] P. T. Dirlam, R. S. Glass, K. Char, J. Pyun, J. Pol. Sci., Part A: Polym. Chem., 55 (2017) 1635-1668.

[11] Y. Xiang, J. Li, J. Lei, D. Liu, Z. Xie, D. Qu, K. Li, T. Deng, H. Tang, ChemSusChem 9 (2016) 3023-3039.

[12] T.-W. Zhang, B. Shen, H.-B. Yao, T. Ma, L.-L. Lu, F. Zhou, S.-H. Yu, Nano Letter 17 (2017) 4894-4901.

[13] J. Zhu, C. Chen, Y. Lu, J. Zang, M. Jiang, D. Kim, X. Zhang, Carbon 101 (2016) 272-280.

[14] Z. Jin, K. Xie, X. Hong, Z. Hu, X. Liu, J.Power Sources 218 (2012) 163-167.

[15] G. Ma, Z. Wen, Q. Wang, C. Shen, J. Jin, X. Wu, J. Mater. Chem. 2 (2014) 19355-19359.

[16] M. Zaccaria, D. Fabiani, G. Cannucciari, C. Gualandi, M. L. Focarete, C. Arbizzani, F. De Giorgio, M. Mastragostino, J. Electrochem.Soc.162 (2015) A915-A920.

[17] Q. Liu, J. Zhu, L. Zhang,Y. Qiu. Renew.Sust. Energ. Rev. 81 (2018) 1825-1858.

[18] J. Zhang, S. Chen, X. Xie, K. Kretschmer, X. Huang, B. Sun, G. Wang, J. Membr. Sci., 472 (2014) 133-140.

[19] A. La Monaca, F. De Giorgio, M. L. Focarete, D. Fabiani, M. Zaccaria, C. Arbizzani, J. Electrochem.Soc. 164 (2017) A6431-A6439.

[20] Z.-M. Huang, Y.-Z. Zhang, M.Kotaki, S.Ramakrishna, Compos. Sci.Technol. 63 (2013) 22233.

[21] N. Bhardwaj, S. C. Kundu, Biotechnol. Adv., 28 (2010) 325-347.

[22] S.-H. Tan, R. Inai, M. Kotaki, S. Ramakrishna, Polymer, 46 (2005) 6128-6134.

[23] S.-S. Choi, Y. S. Lee, C. W. Joo, S. G. Lee, J. K. Park, K.-S. Han, Electrochim. Acta 50 (2004) 339-343.

[24] C. M. Costa, J. L. Gomez Ribelles, S. Lanceros-Méndez, G. B. Appetecchi, B. Scrosati, J. Power Sources 245 (2014) 779-789.

[25] X. Zuo, J. Wu, X. Ma, X. Denga, J. Cai, Q. Chen, J. Liu, J. Nan, J. Power Sources 407 (2018) 44-52.

[26] M.- H. Ryou, Y. M. Lee, J.- K. Park, J. W. Choi, Adv. Mater., 23 (2011) 3066-3070.

[27] R. Pan, X. Xu, R. Sun, Z. Wang, J. Lindh, K. Edström, M. Strømme, L. Nyholm, Small 14 (2018) 1704371 (1-9).

[28] J. Q. Huang, T. Z. Zhuang, Q. Zhang, H. J. Peng, C. M. Chen, F. Wei, ACS Nano 9 (2015) 3002-3011.

[29] C. Wang, K. Su, W. Wan, H. Guo, H. Zhou, J.Chen, X. Zhangb, Y. Huang J. Mater. Chem., 2 (2014) 5018-5023.

[30] W. Jang, J. Yun, K. Jeon, and H. Byun, RSC Adv. 5 (2015) 46711-46717.

[31] T.- Z. Zhuang, J.- Q. Huang, H.-J. Peng, L.- Y. He, X.- B. Cheng, C.- M. Chen, Q. Zhang, Small 12 (2016) 381-389.

[32] M. Alcoutlabi H. Lee J.V. Watson X. Zhang, J. Mater.Sci., 48 (2013) 2690-2700.

[33] M. Schmidt, U. Heider, A. Kuehner, R. Oesten, M. Jungnitz, N. Ignat'ev, P. Sartori, J. Power Sources 97 (2001) 557-560.

[34] A. La Monaca, F. De Giorgio, F. Soavi, G. Tarquini, M. Di Carli, P. P. Prosini, C. Arbizzani, ChemElectroChem, 2 (2018) 1272-1278.

[35] R.D. Rauh, F. S. Shuker, J.M. Marston, S.B. Brummer, J. Inorg. Nucl. Chem., 39 (1977) 1761-1766.

[36] G. Tarquini, M. Di Carli, L. D. Seta, M. Moreno, P.P. Prosini, Solid State Ionics, 317 (2018) 170-174.

[37] Y. Bormashenko, R. Pogreb, O. Stanevsky, E. Bormashenko, Polym. Test., 23 (2004) 791-796.

[38] Q. Zou, Y.-C. Lu, J. Phys. Chem. Letter, 7 (2016) 1518-1525.

[39] B. Wu, J. Lochala, T. Taverne, J. Xiao, Nano Energy 40 (2017) 34-41.

[40] G. Bieker, M. Winter, P. Bieker, Phys. Chem. Chem. Phys. 17 (2015) 8670-8679.

Figure captions

Figure 1. SEM images of the sample E1 (5 min spinning time): a-c) surface images at different magnifications, d) electrospun PVdF/GO layer detached from Celgard membrane, e-f) cross-sections.

Figure 2. Dielectric strength tests on pristine Celgard, on E1 membrane before and after PVdF/GO layer peeling off.

Figure 3. a) FTIR-ATR spectra of PVdF/GO/Celgard separator (S1CT, red) and of pristine Celgard (black).

Figure 4. EIS spectra (10 points/decade) of the SS/LP30-soaked separator/SS cells, with the magnification of the high frequency region (on the right). The highest frequency is 200 kHz, and the points at 10 kHz are indicated by a circle.

Figure 5. UV-VIS spectra of the solution containing permeated polysulfides after 1 hour.

Figure 6. Potential profiles of the WE and CE of Li//Li cells with different separators during galvanostatic stripping/deposition cycles at 0.75 mA cm^{-2}. The duration of each cycle was 2 hours and the cut-off potentials of the electrodes were set to -0.5 V and 0.5 V vs Li^{+}/Li.

Figure 7. Impedance spectra (100 kHz- 100 mHz) of the Li//Li cells with a) 2-E1, b) 2-E1p and c) C-E1p symmetric separators before and after the galvanostatic tests of Figure 6. The insets show the high-frequency part of the spectra.

Figure 8. SEM images displaying the dendrite growth on a) lithium WE, facing the PVdF/GO electrospun layer of an E1p separator, and b) lithium CE of a Li//Li symmetric cell; scheme of the dendrite growth on c) WE and d) CE.

Figure 9. 1^{st} (solid lines) and 10^{th} (dotted lines) galvanostatic charge/discharge cycles at C/10 of cells with E1 (red), S5C (black) and Celgard (blue) separators.

Figura 10. Potential profiles of the anode (black) and of the cathode (red) during the first 3

galvanostatic cycles at C/8 of the cell with E1p with the electrospun layer faced to Li anode.

Table 1

Table 1. Resistivity of the electrolyte-soaked separators and MacMullin number (N_M)

Samples	Thickness μm	Resistivity ohm cm (LP30)	N_M (LP30)	Resistivity ohm cm (DD)	N_M (DD)
LP30		82.50 [33]	1		
DD				249.25 [34]	1
Celgard	25 μm	1438	17	2355	10
E1	30 μm	1667	20	2015	8
E1p	30 μm			1518	6
S1C	29 μm	2000	24		
S1CT	28 μm	2820	34	2110	9
S2C	30 μm	1660	20		
S2CT	27 μm	2847	35		
S5C	30 μm	2310	28	2620	11
S5CT	31 μm	1790	22		

Figure 1

Click here to download high resolution image

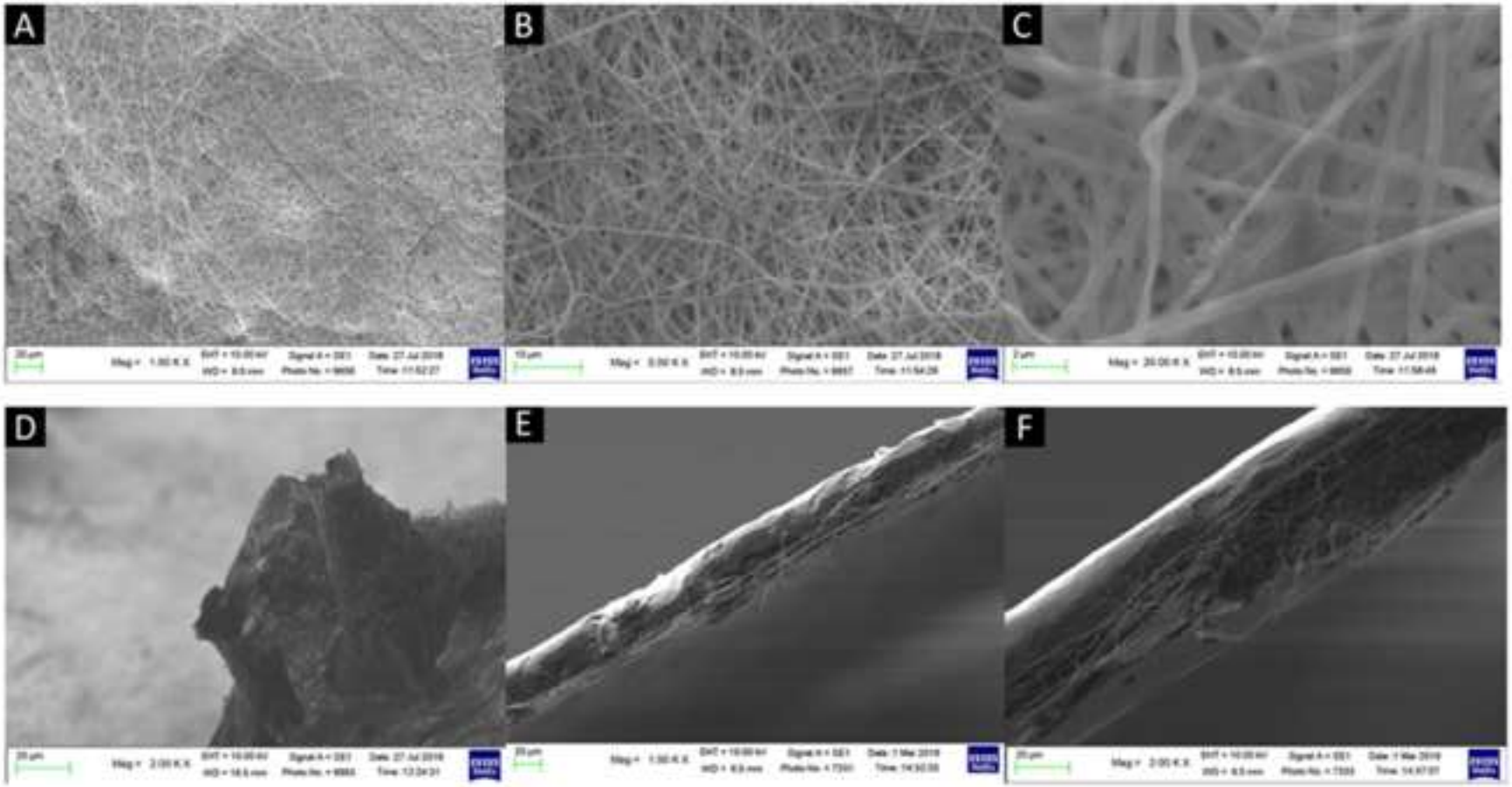

Figure 2

Click here to download high resolution image

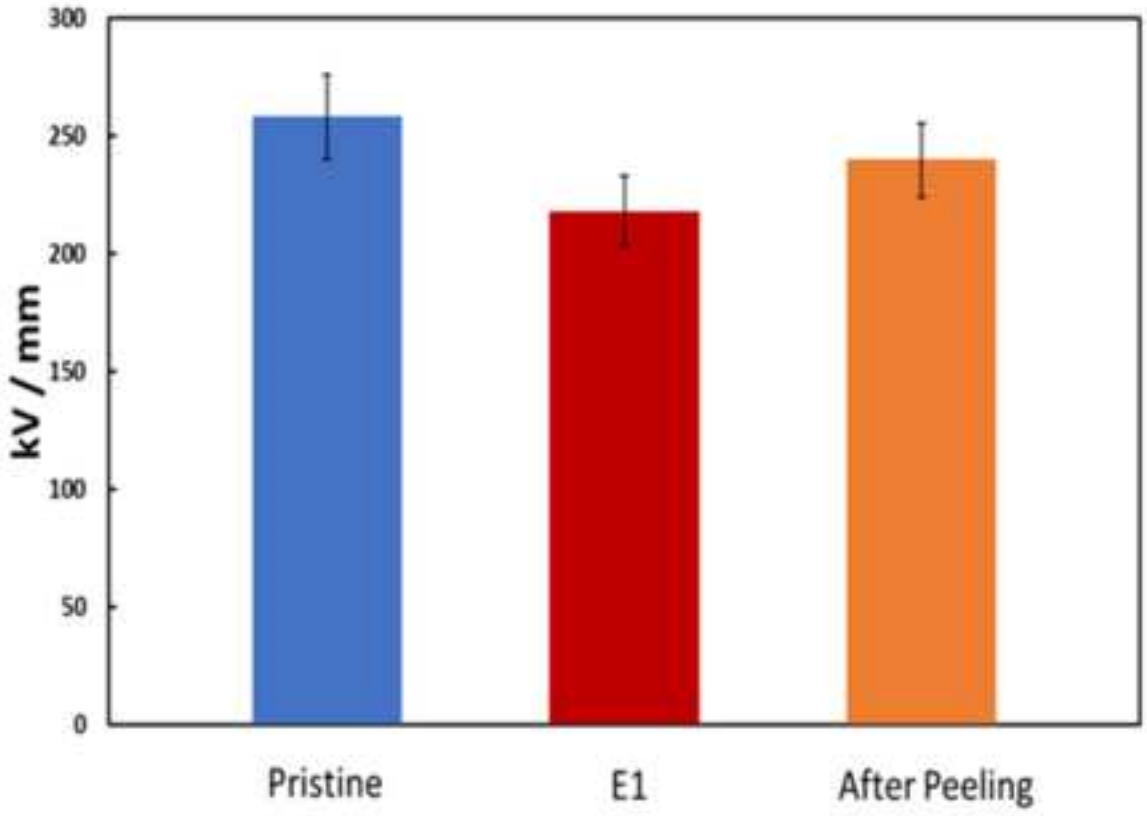

Figure 3

Click here to download high resolution image

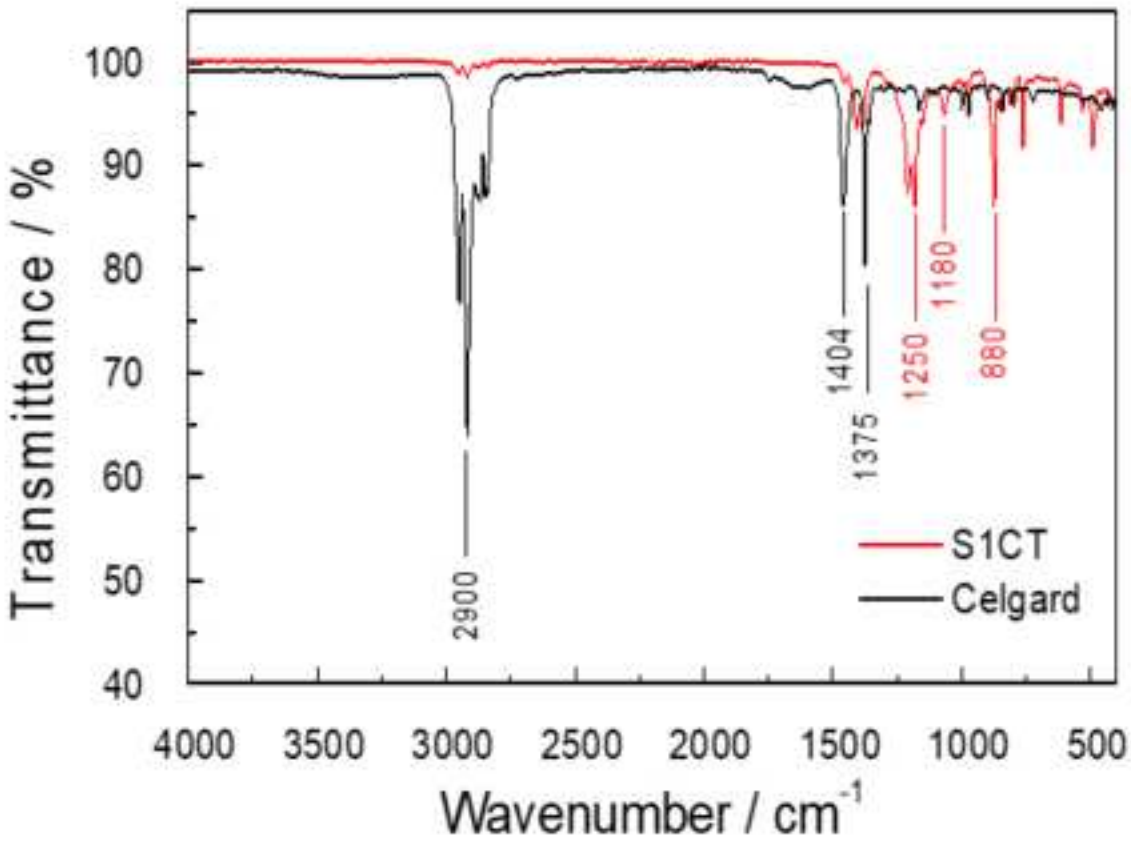

Figure 4

Click here to download high resolution image

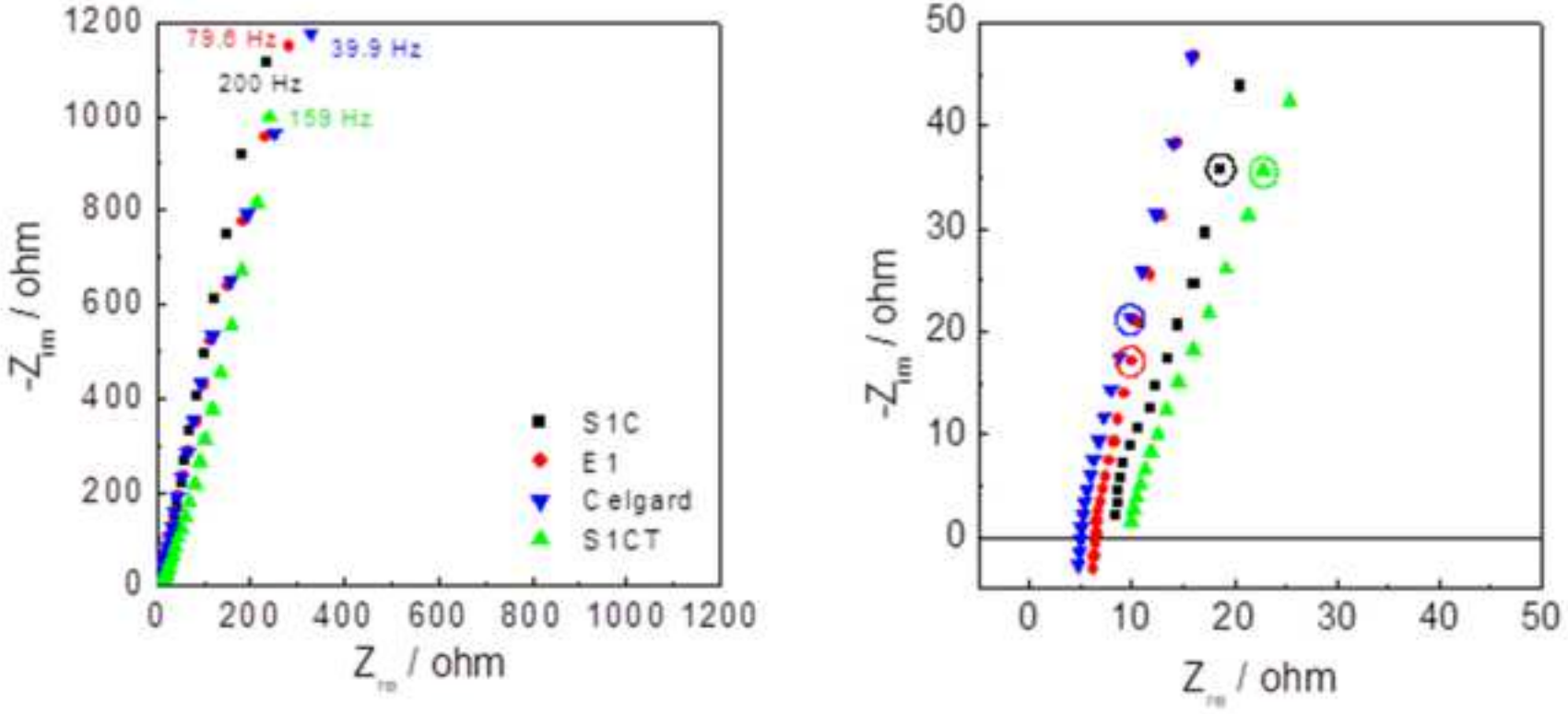

Figure 5

Click here to download high resolution image

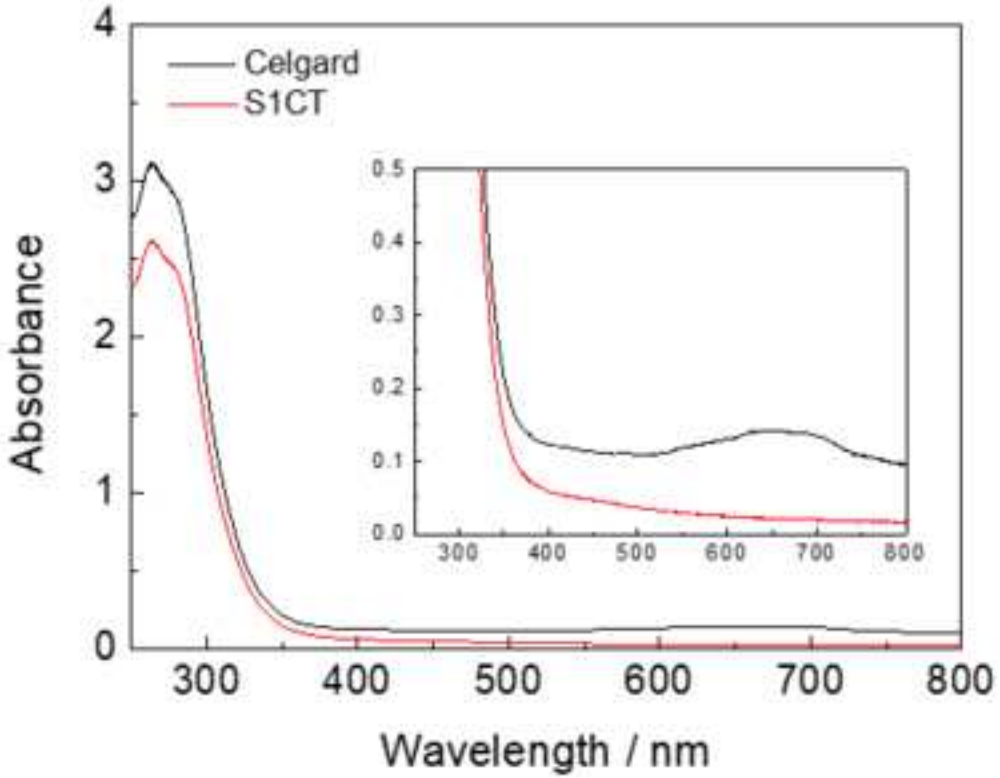

Figure 6

Click here to download high resolution image

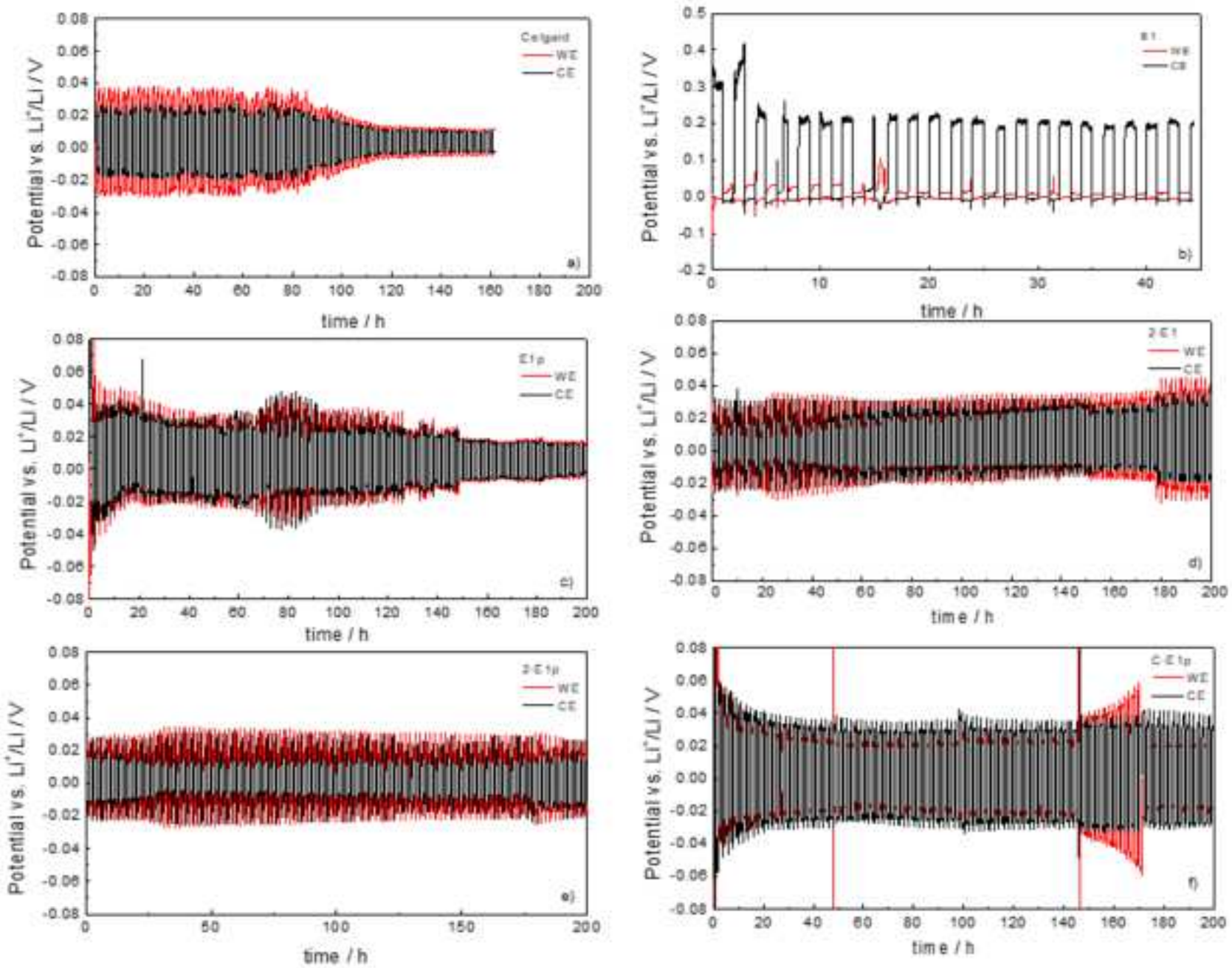

Figure 7

Click here to download high resolution image

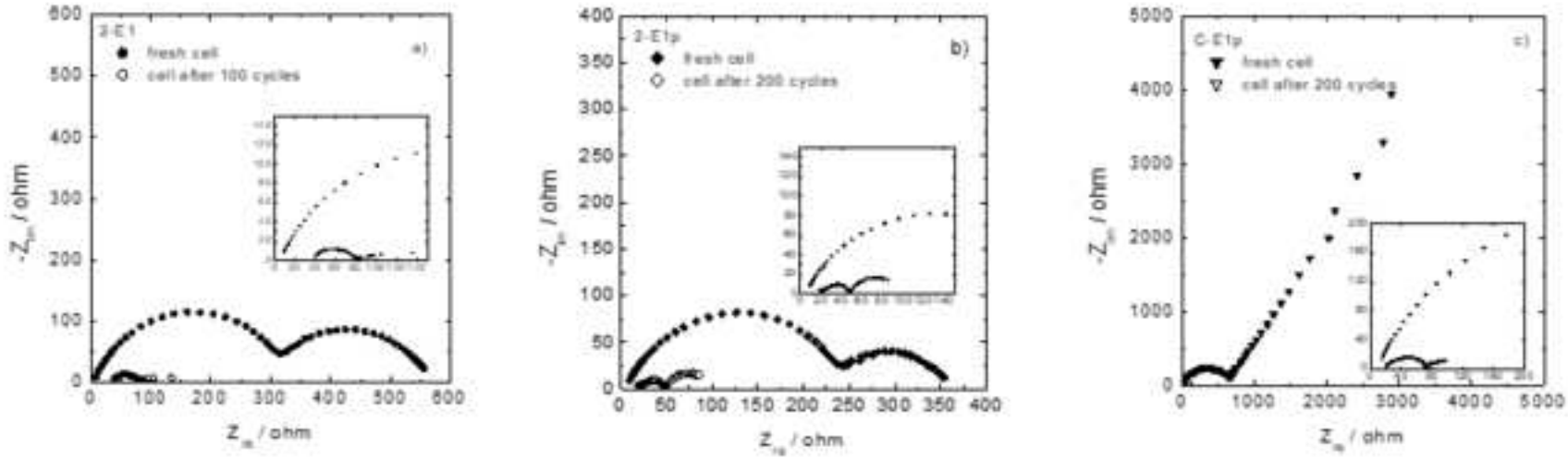

Figure(s) - provided separately

Click here to download high resolution image

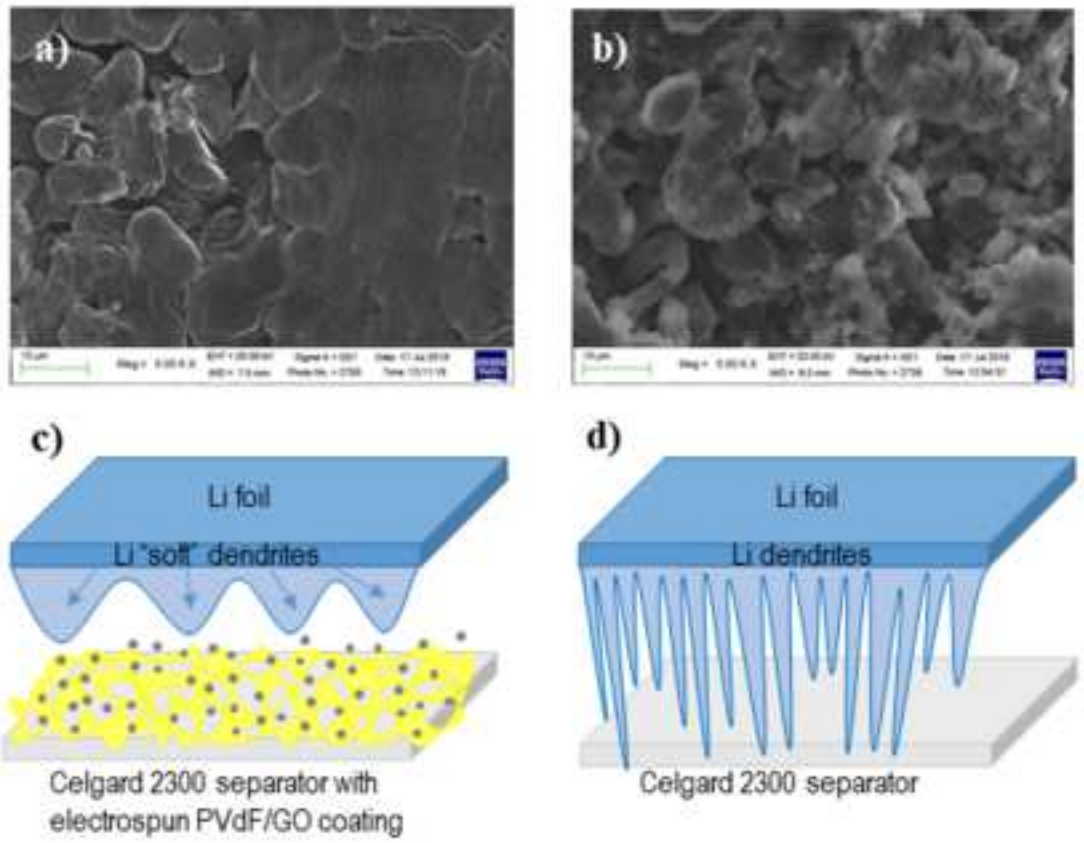

Figure(s) - provided separately

Click here to download high resolution image

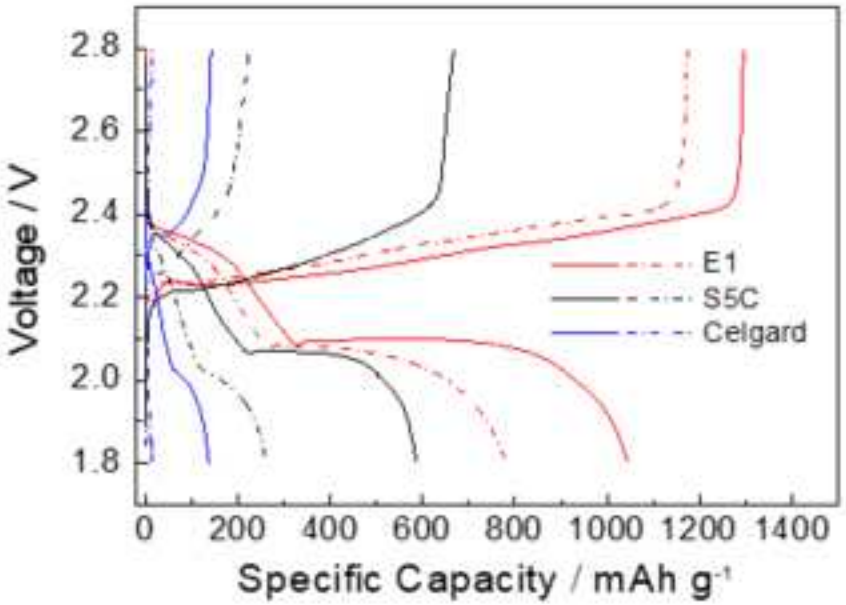

Figure(s) - provided separately
Click here to download high resolution image

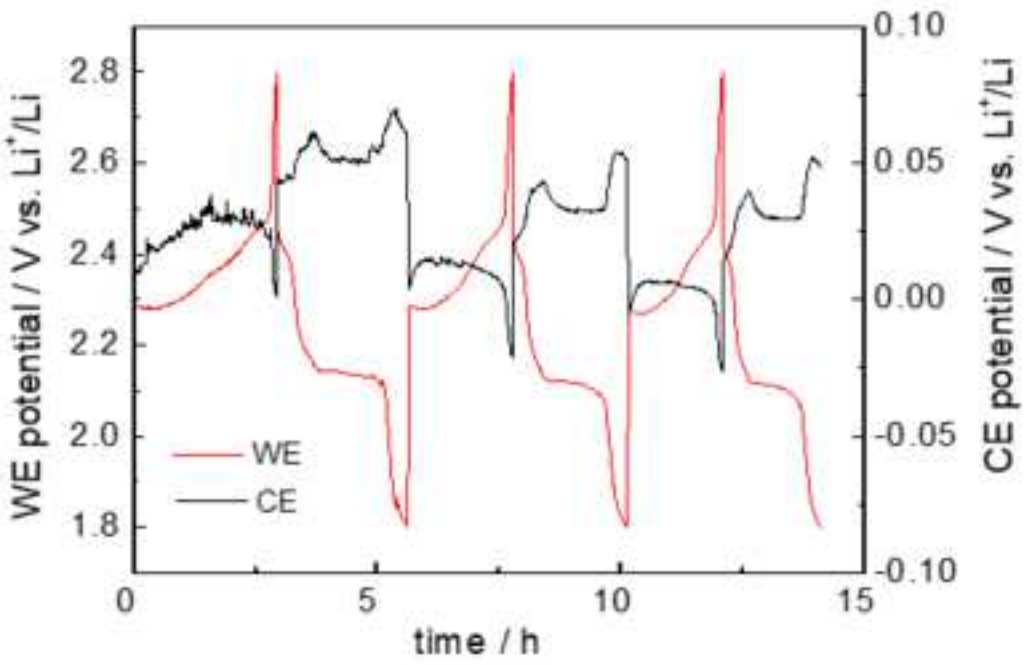

Supplementary Materials

Click here to download Supplementary Materials: Supplementary Information_151119.docx

***Declaration of Interest Statement**

Declaration of interests

☒ The authors declare that they have no known competing financial interests or personal relationships that could have appeared to influence the work reported in this paper.

☐The authors declare the following financial interests/personal relationships which may be considered as potential competing interests: